Chemical Physics 419 (2013) 156–162

Contents lists available at SciVerse ScienceDirect

Chemical Physics

journal homepage: www.elsevier.com/locate/chemphys

# Three-pulse multiplex coherent anti-Stokes/Stokes Raman scattering (CARS/CSRS) microspectroscopy using a white-light laser source

Kotatsu Bito [a,b], Masanari Okuno [a], Hideaki Kano [c,a], Philippe Leproux [d,e], Vincent Couderc [d], Hiro-o Hamaguchi [a,f,*]

[a] Department of Chemistry, School of Science, The University of Tokyo, 7-3-1 Hongo, Bunkyo-ku, Tokyo 113-0033, Japan
[b] Analytical Science Research Laboratories, Kao Corporation, 2606 Akabane, Ichikai-Machi, Haga-Gun, Tochigi 321-3497, Japan
[c] Institute of Applied Physics, University of Tsukuba, 1-1-1 Tenodai, Tsukuba, Ibaraki 305-8573, Japan
[d] Institut de Recherche XLIM, UMR CNRS No. 7252, 123 Avenue Albert Thomas, 87060 Limoges Cedex, France
[e] LEUKOS, ESTER Technopole, 1 Avenue d'Ester, 87069 Limoges Cedex, France
[f] Institute of Molecular Science and Department of Applied Chemistry, National Chiao Tung University, 1001 Ta Hsueh Road, Hsinchu 300, Taiwan

ARTICLE INFO

*Article history:*
Available online 15 February 2013

*Keywords:*
Raman
Coherent Raman
Vibrational spectroscopy
Microspectroscopy
Nonlinear spectroscopy

ABSTRACT

We have developed a three-pulse non-degenerate multiplex coherent Raman microspectroscopic system using a white-light laser source. The fundamental output (1064 nm) of a Nd:YAG laser is used for the pump radiation with the white-light laser output (1100–1700 nm) for the Stokes radiation to achieve broadband multiplex excitations of vibrational coherences. The second harmonic (532 nm) of the same Nd:YAG laser is used for the probe radiation. Thanks to the large wavelength difference between the pump and probe radiations, coherent anti-Stokes Raman scattering (CARS) and coherent Stokes Raman scattering (CSRS) can be detected simultaneously. Simultaneous detection of CARS and CSRS enables us to obtain information on the electronic resonance effect that affects differently the CARS and CSRS signals. Simultaneous analysis of the CARS and CSRS signals provides us the imaginary part of $\chi^{(3)}$ without introducing any arbitrary parameter in the maximum entropy method (MEM).



## 1. Introduction

Time- and space-resolved molecular information on organs, tissues and cells is vitally important for understanding life. Microspectroscopic techniques based on Raman spectroscopy provide such information from unlabeled or unstained biological systems in a nondestructive and noninvasive fashion [1–11]. Hence, various bio-molecular systems have been investigated with the use of Raman microspectroscopy [12–18].

Thanks to the recent advances in light source technologies, various coherent Raman microspectroscopic techniques have been developed for bio-imaging such as coherent anti-Stokes Raman scattering (CARS) microscopy [2,3], stimulated Raman scattering (SRS) microscopy [7,8] and optical heterodyne-detected Raman-induced Kerr effect (OHD-RIKE) microscopy [9]. These techniques employ a set of two narrow-band laser pulses (pump- and Stokes- or $\omega_1$- and $\omega_2$-lasers) for exciting a particular vibrational band, typically a CH stretch band, to perform video-rate vibrational imaging. However, these techniques are difficult to apply to vibrational imaging in the fingerprint region, where vibrational bands are much more congested and are hard to be resolved from one another. In order to overcome this difficulty, broadband multiplex CARS microspectroscopy has been developed recently [4,6,10]. CARS microspectroscopy using a nanosecond supercontinuum light source (or white-light laser source) provides CARS spectra and images from the whole fundamental vibrational bands including CH stretches and fingerprint bands [10,18]. Broadband multiplex CARS microspectroscopy enables us to perform fast, quantitative and multi-vibrational mode imaging of biological samples such as living cells and tissues.

The electronic resonance Raman process enhances Raman intensities. Coherent Raman spectroscopy with electronic resonance has been established as a highly sensitive method in molecular spectroscopy [19–22]. The signal enhancement by electronic resonance lowers the detection limit from several tens of millimolar to several tens of micro-molar [21]. Since the CARS signal is blue-shifted from the excitation laser and has a well-defined unidirectional wave vector, resonance CARS is more advantageous than spontaneous resonance Raman for spectral and spatial separation of the fluorescence background. So far, the resonance CARS technique has been employed for investigation of biological dye, pigments and chromophores such as cytochrome *c* [19,21] and

* Corresponding author. Address: Institute of Molecular Science and Department of Applied Chemistry, College of Science, National Chiao Tung University, 1001 Ta Hsueh Road, Hsinchu 300, Taiwan. Tel.: +886 3 5712121x56504.
*E-mail address:* hhama@nctu.edu.tw (H. Hamaguchi).

0301-0104/$ - see front matter © 2013 Elsevier B.V. All rights reserved.
http://dx.doi.org/10.1016/j.chemphys.2013.02.007

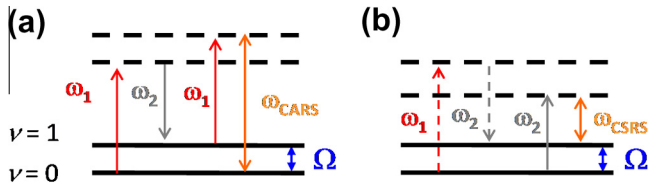


**Fig. 1.** Diagrams for (a) CARS, $\omega_{CARS} = 2\omega_1 - \omega_2$ and (b) CSRS, $\omega_{CSRS} = 2\omega_2 - \omega_1$. $\omega_1 - \omega_2 = \Omega$ denotes a vibrational frequency and $v$ the vibrational quantum number.

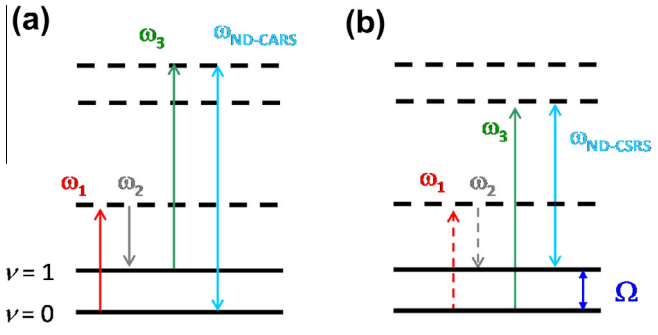


**Fig. 2.** Diagrams for (a) nondegenerate CARS, $\omega_{CARS} = \omega_1 - \omega_2 + \omega_3$ and (b) nondegenerate CSRS, $\omega_{CSRS} = -\omega_1 + \omega_2 + \omega_3$. $\omega_1 - \omega_2 = \Omega$ denotes a vibrational frequency and $v$ the vibrational quantum number.

β-carotene [21] in solution. Recently, resonance CARS signal under a microscope has also been reported [23–25].

In the present study, we develop a resonance CARS microspectroscopic system using a white-light laser source. We show that, in addition to CARS, we can also detect the coherent Stokes Raman scattering (CSRS) signal simultaneously using a three laser nondegenerate CARS/CSRS setting. Fig. 1 shows schematics of the CARS (a) and CSRS (b) processes. CSRS is one of the third-order nonlinear processes analogous to CARS [26,27]. The CARS and CSRS spectra are theoretically identical with each other under an electronic nonresonant condition [26,27]. On the other hand, these spectra become different if electronic resonance comes into play [28,29]. Owing to this nature, the quantitative information on the electronic resonance effect can be obtained through a simultaneous analysis of CARS and CSRS spectra.

In general, it is difficult to obtain both CARS and CSRS spectra simultaneously, because the CSRS signal is red-shifted from the pump (and probe) radiation, and thus spectrally overlapped with the Stokes radiation in the case of the two-pulse coherent Raman process. This difficulty is overcome by introducing the probe laser with a different color from the pump laser [30,31]. Fig. 2 shows schematics of the three-pulse (non-degenerate) CARS (a) and CSRS (b) processes with the pump ($\omega_1$), Stokes ($\omega_2$), and probe ($\omega_3$) laser pulses. If $\omega_3$ is not equal to $\omega_1$, both the CARS and CSRS can be spectrally separated from the three incident laser radiations. Using a broadband laser source for the Stokes ($\omega_2$) radiation, multiplex CARS and CSRS processes take place as shown in Fig. 3 [6,10]. With use of the third probe radiation ($\omega_3$), the broadband CARS and CSRS spectra are obtained simultaneously at $\omega_{CARS} = \omega_1 - \omega_2 + \omega_3$ and $\omega_{CSRS} = -\omega_1 + \omega_2 + \omega_3$. The phase matching conditions ($\boldsymbol{k}_{CARS} = \boldsymbol{k}_1 - \boldsymbol{k}_2 + \boldsymbol{k}_3$ and $\boldsymbol{k}_{CSRS} = -\boldsymbol{k}_1 + \boldsymbol{k}_2 + \boldsymbol{k}_3$, where $\boldsymbol{k}_x$ corresponds to the wave vector of $\omega_x$-laser [26]) are simultaneously satisfied by using a microscope objective with high numerical aperture [14,16]. The three-pulse (non-degenerate) CARS and CSRS spectra can thus be obtained at the same position/time under a microscope.

## 2. Experimental

The experimental setup is shown in Fig. 4. We used three laser pulses with different colors, pump ($\omega_1$), Stokes ($\omega_2$) and probe ($\omega_3$). The laser source was a sub-ns microchip Nd:YAG laser (center wavelength 1064 nm, temporal duration 800 ps, repetition rate 33 kHz). A portion of the fundamental output was used for the pump pulse ($\omega_1$). The second portion was used as a seed for generating supercontinuum or white-light laser, (spectral range is 400–1700 nm) [10]. In the present setup, only the near infrared (NIR) spectral component of the white-light laser was used for the Stokes pulse ($\omega_2$). The spectral profile of the Stokes laser is shown in Fig. 5. It covered the spectral region of 1100–1700 nm. The third portion of the fundamental output was frequency-doubled by a KTP crystal to generate the second harmonic (532 nm) used for probe pulse ($\omega_3$). The $\omega_1$-, $\omega_2$-, and $\omega_3$-laser powers were <30 mW,<20 mW and <5 mW, respectively. Three laser beams were superimposed collinearly using a dual (532/1064 nm) notch filter, and then introduced into a custom-made microscope (Nikon). They were tightly focused onto the sample with a 40×, 0.9 NA microscope objective. The CARS and CSRS signals were collected by a 40×, 0.6 NA microscope objective in the forward detection. They were spectrally filtered with a dual (532/1064 nm) notch filter, and then guided into a polychromator (HORIBA Jobin-Yvon, *i*HR 320, Grating: 300 grooves/mm). Finally, the CARS and CSRS signals were detected by a CCD camera (Andor Technology, Newton 920P BRDD). Since narrow-band ns-probe pulses were used for $\omega_1$ and $\omega_3$, the spectral resolution was determined primarily by the spectrometer. The spectral resolution was <30 $cm^{-1}$. In order to obtain a microscopic image, the sample was placed on a piezo-driven *xyz* translator (MadCity, NanoLP-100). The CARS and CSRS spectra were measured by point-by-point acquisition at each sample position. The samples were sandwiched with a cover slip and a single concave microscope slide glass. For the sake of intensity correction, the CARS and CSRS spectra were divided by a non-resonant background [30], which was measured from the underneath cover slip under the same experimental conditions.

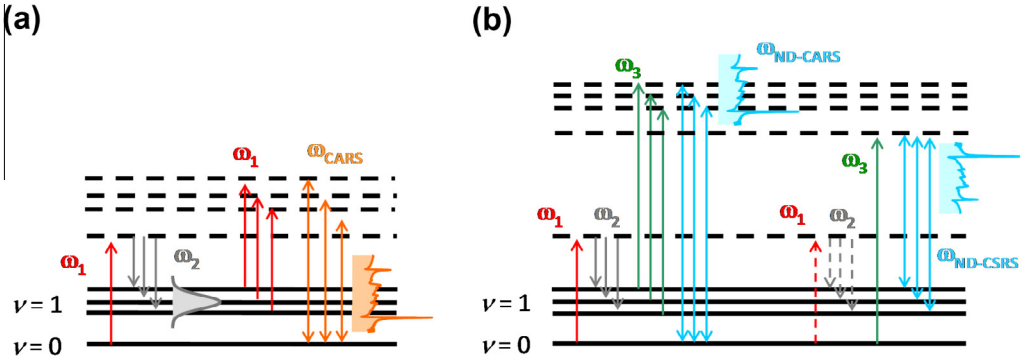


**Fig. 3.** Diagrams for broadband multiplex (a) CARS and (b) nondegenerate CARS and CSRS.

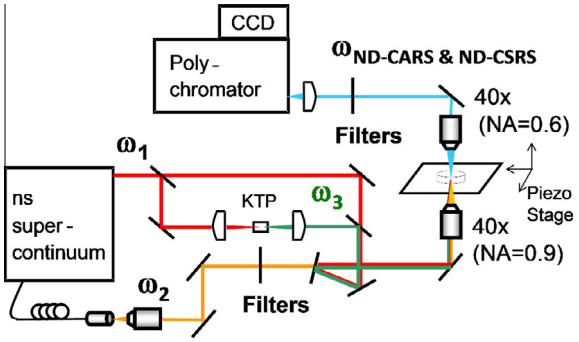


**Fig. 4.** A schematic diagram of the setup of the broadband multiplex CARS/CSRS microspectroscopy.

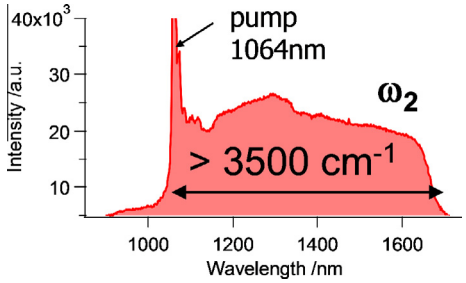


**Fig. 5.** SC spectrum obtained with a NIR spectrometer (intensity uncorrected). The CARS/CSRS spectral coverage (wavenumber difference between the pump and SC) is >3500 $cm^{-1}$.

## 3. Results and discussion

### 3.1. Resonance CARS and CSRS spectroscopy

Fig. 6 shows the multiplex CARS and CSRS spectra of neat toluene. The intensity is corrected as described in Section 2. The negative and positive Raman shifts correspond to CARS and CSRS, respectively. The spectral coverage is over 3000 $cm^{-1}$ both in CARS and CSRS. The CARS spectral profile is similar to that of CSRS, indicating that there is no electronic resonance effect for neat toluene with 532-nm probe.

Fig. 7a shows the multiplex CARS and CSRS spectra of 10-mM toluene solution of β-carotene. It is clear that the CARS signal is much stronger than CSRS. This asymmetry is due to the electronic resonance effect of β-carotene, which has an electronic absorption band around 490 nm (Fig. 7b). The vibrationally nonresonant signal with a broad spectral profile is also stronger in the CARS side than that in the CSRS side due to the electronic resonance enhancement [14,16,32,33]. The resonance enhancement takes place when the photon energy of the excitation laser approaches the electronic transition energy [26,27]. The electronic resonance effect manifests itself as the intensity ratio between the CARS and CSRS signals. If we map the integrated CARS/CSRS intensity ratio at each sample point, we can spotlight and differentiate the chromophore distributions from those of other non-absorbing molecules like lipids and proteins in biological samples. Various kinds of chromophores, carotenoids, hemeproteins and so on, show absorption bands in the present spectral region. Resonance CARS/CSRS imaging will introduce a new axis of bio-imaging with otherwise unobtainable information on the electronic resonances of chromophores.

### 3.2. New phase retrieval method using CARS and CSRS signals

The CARS process is described by the third-order nonlinear susceptibility, $\chi^{(3)}$. Another $\chi^{(3)}$ process, the so-called nonresonant

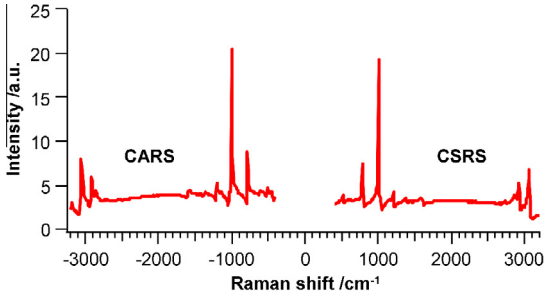


**Fig. 6.** The broadband multiplex CARS/CSRS spectrum of neat toluene.

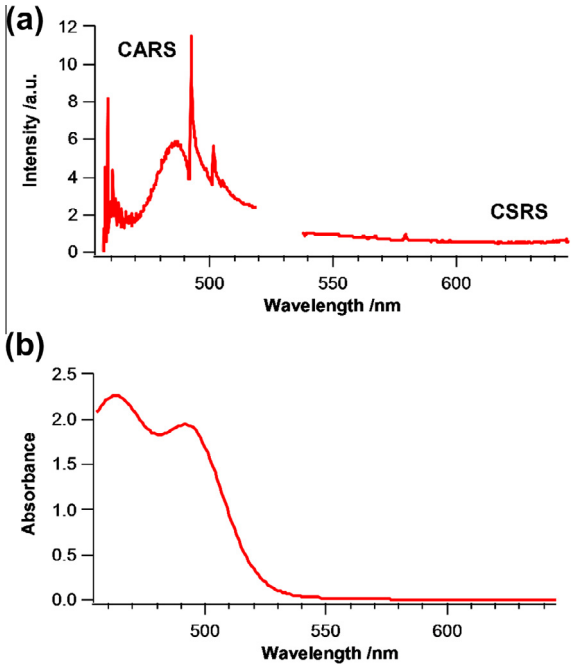


**Fig. 7.** (a) The broadband multiplex CARS/CSRS spectrum and (b) absorption spectrum of β-carotene in toluene.

background, is also overlapped with the CARS spectra. The overall spectral profile becomes in general dispersive due to the interference between the CARS (vibrationally resonant component, $\chi_R^{(3)}$) and NRB (vibrationally nonresonant component, $\chi_{NR}^{(3)}$) [26,27] as in the following:

$$I_{CARS} \propto |\chi_R^{(3)} + \chi_{NR}^{(3)}|^2 = |\chi_R^{(3)}|^2 + 2\chi_{NR}^{(3)}\mathrm{Re}[\chi_R^{(3)}] + |\chi_{NR}^{(3)}|^2. \quad (1)$$

The resonant part of $\chi^{(3)}$ is written as,

$$\chi_R^{(3)} = \sum_j \frac{A_j}{\Omega_j - (\omega_1 - \omega_2) - i\Gamma_j}. \quad (2)$$

Here $A_j$ is the CARS amplitude, $\Omega_j$ the $j^{th}$ vibrational frequency and $\Gamma_j$ the bandwidth of the $j^{th}$ Raman mode. Ordinary (spontaneous) Raman intensity corresponds to the imaginary part of $\chi^{(3)}$. Phase information of $\chi^{(3)}$ in Eq. (2) is needed in order to compare the CARS spectrum with the spontaneous Raman, which is linear to molecular concentration and is more tractable for analysis. In order to obtain this phase information, various experimental and mathematical approaches have been examined [14,16,34]. In our previous studies, we employed the maximum entropy method (MEM) [10,35–37]. In MEM, an autocorrelation function obtained from a measured coherent Raman spectrum is extrapolated to

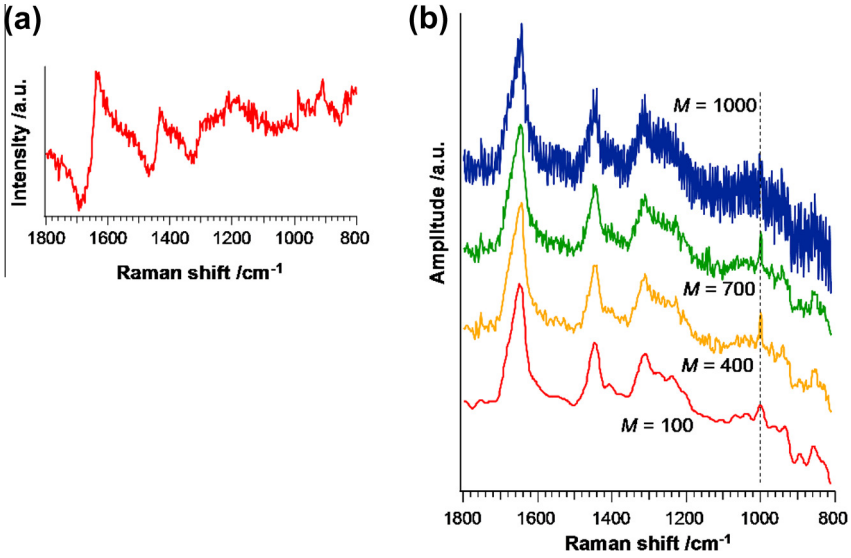


**Fig. 8.** (a) A CARS spectrum of a hair and (b) retrieved Im[$\chi^{(3)}$] spectra with different orders of pole $M$. The dash line in Fig. 8b indicates 1003 cm$^{-1}$.

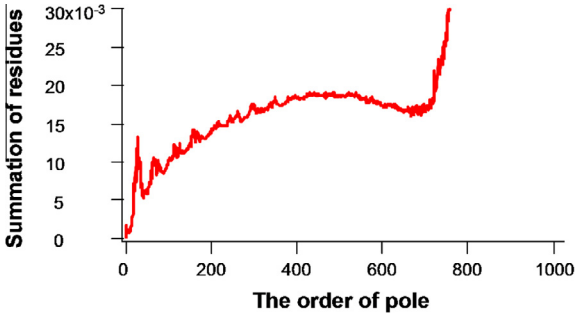


**Fig. 9.** The order of pole dependence of the difference between the Im[$\chi^{(3)}$] spectra obtained from CARS and CSRS of ethanol solution. The data points were $N = 1024$.

maximize the information entropy with a fixed maximum lag, the order of pole, as a parameter [36,37]. This feature enables us to retrieve Im[$\chi^{(3)}$] with high spectral resolution by means of a finite frequency range. The MEM analysis, however, has one arbitrary parameter, the order of pole ($M$), which should be smaller than the number of sampled points ($N$). The spectral resolution and contribution of the high-frequency noise depend on $M$. Namely, if $M$ is smaller (larger), the spectral resolution is more (less) degraded and the high-frequency noise is more (less) reduced.

Typical dependence of the retrieved Im[$\chi^{(3)}$] spectra on $M$ is shown in Fig. 8 for the CARS spectrum of a hair sample. For $M/N = 100/1340$, the spectral profile contains lower noise but shows a spectral degradation. In particular, the peak at 1003 cm$^{-1}$, which corresponds to the phenylalanine (Phe) residue, is broader than those of the spectra with higher $M$. The bandwidth of Phe is about 5 cm$^{-1}$ for $M = 1000$. This value approximately corresponds to the spectral resolution of the present experimental system. Since the bandwidth of Phe is much smaller than the instrumental spectral resolution, the retrieved Im[$\chi^{(3)}$] spectrum is not broadened for $M > 400$. On the other hand, in the cases of $M = 1000$, high-frequency artificial noise contributes to the spectral profile. In order to obtain the optimum value of $M$, we need further independent spectral information. CSRS provides such information as shown below.

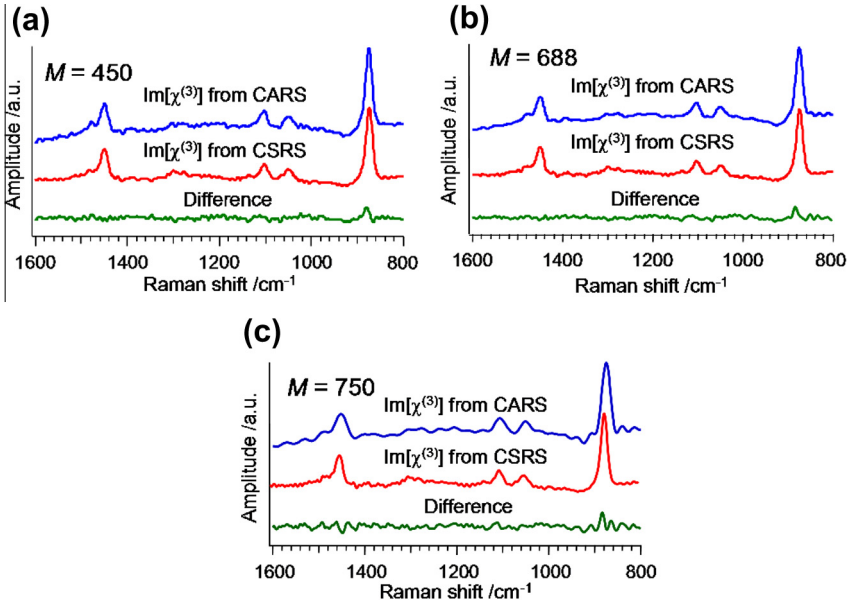


**Fig. 10.** (a) The retrieved Im[$\chi^{(3)}$] spectra of ethanol solution for $M = 450$ and their difference Im[$\chi^{(3)}$] spectrum; (b) $M = 688$; (c) $M = 750$.

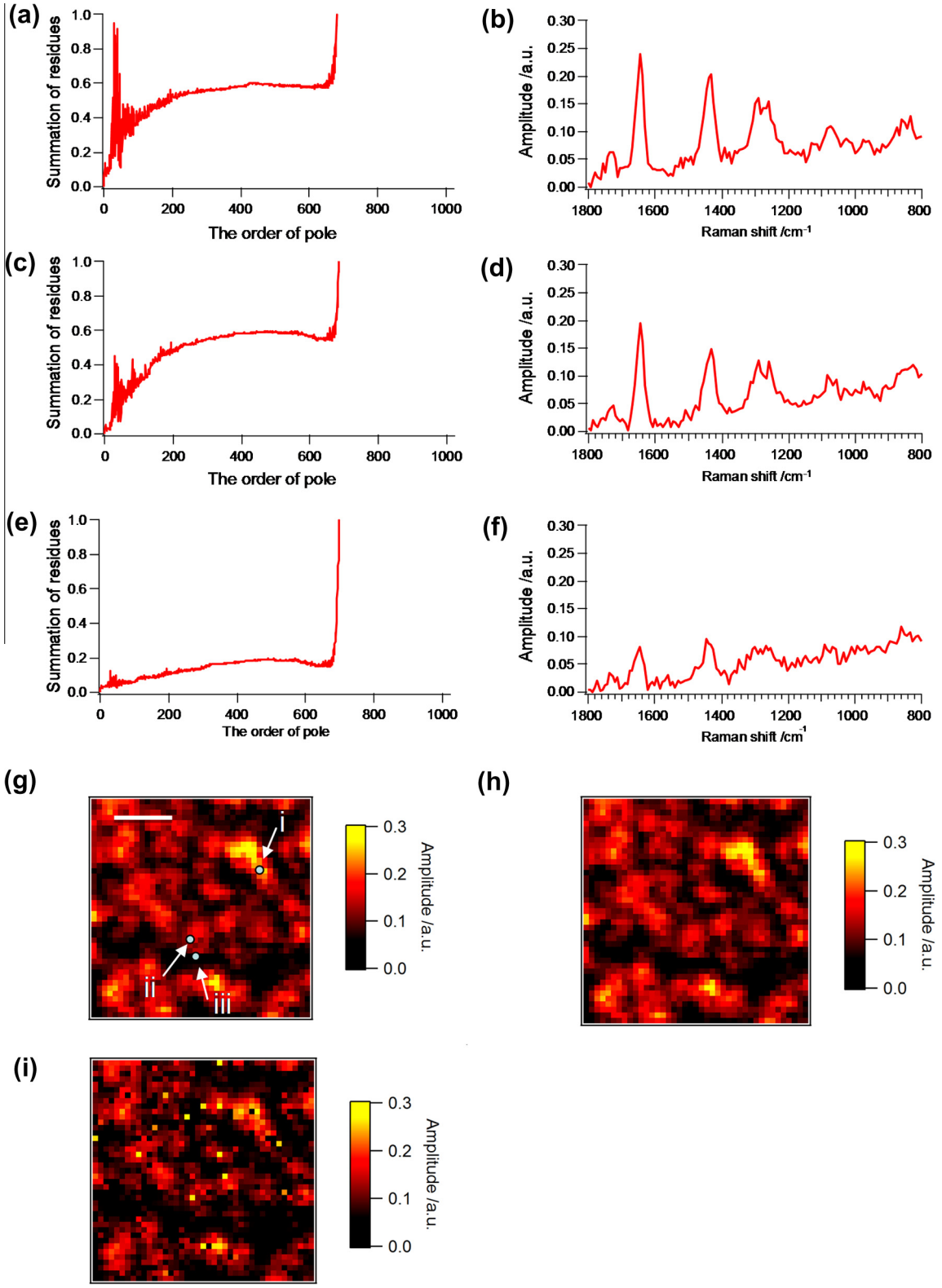


**Fig. 11.** (a), (c), and (e) show the results of $M$-dependence of the sum of amplitude difference between the retrieved $\mathrm{Im}[\chi^{(3)}]$ spectra of CARS and CSRS for three different positions at the sample which correspond to i, ii, and iii indicated in Fig. 12g, respectively; (b), (d), and (f) show the retrieved $\mathrm{Im}[\chi^{(3)}]$ spectra for $M = 630$ which correspond to Fig. 12a, c, and e, respectively; (g) the image was constructed for the CH bend modes (1420–1460 $\mathrm{cm}^{-1}$) at the fixed value of $M = 630$; (h) $M = 340$; (i) $M = 750$. The scale bar corresponds to 10 μm. The exposure time for each pixel was 200 ms, and each image consists of 41 × 41 pixels, corresponding to 20 × 20 μm. Overall measurement time was approximately 5 min.

Under an electronic nonresonant condition, the $\mathrm{Im}[\chi^{(3)}]$ spectra obtained from the CARS and CSRS processes should be identical with each other [26,27]. Therefore, CSRS provides independent experimental information on a spectrum that should be exactly the same as the corresponding CARS spectrum. The optimum value of $M$ can be determined by minimizing the difference between the

retrieved Im[$\chi^{(3)}$] CARS and CSRS. The results of a proof-of-principle experiment using solvent are shown in Fig. 9. The spectrum ($N$ = 1024) of ethanol is analyzed with the MEM for different values of $M$ [35,36]. Since ethanol has no electronic resonance under the present experimental condition, the spectral profile retrieved from the CARS and CSRS should be identical with each other. We evaluate the amplitude differences at 1024 points between the retrieved CARS and CSRS Im[$\chi^{(3)}$] spectra in the region of 800–1600 cm$^{-1}$. Fig. 9 shows the $M$-dependence of the sum of the 1024 amplitude differences between the retrieved CARS and CSRS Im[$\chi^{(3)}$] spectra. It shows a minimum around $M$ = 688. The retrieved Im[$\chi^{(3)}$] spectra for $M$ = 450, 688, and 750 are shown in Fig. 10a–c. As the value of $M$ increases, artificial noise due to MEM analysis becomes prominent. It originates from the oscillatory structures in the CARS and CSRS spectra. The period of the oscillatory structure in CARS is longer than that in CSRS. They are presumably caused by the difference in the detected wavelength region (CARS: approximately 490–510 nm, and CSRS: approximately 555–580 nm). It is clear that the spectral profile for $M$ = 688 gives the best of the three. So far, in the MEM analysis, the order of $M$ has been empirically determined in advance such as the value from $N$/3 to $N$/2 [38] to suppress the high-frequency artificial noise. In the present analysis, we employ a value of $M$ ($M$ = 0.67$N$) that is larger than empirically used values. It means that the optimum value can be found by taking into account the spectral resolution and the noise reduction simultaneously.

This new technique of MEM is applied to the CARS and CSRS spectral imaging. The sample is oil-in-water (O/W) emulsion. A commercially available mayonnaise is used. Fig. 11a, c, and e show the results of $M$-dependence of the sum of amplitude differences between the retrieved CARS and CSRS Im[$\chi^{(3)}$] spectra for three different positions in the sample. Although the signal intensities are different from the three points, the dependence shows a minimum around $M$ = 630. Based on the $M$-dependence, we fix the value of $M$ to 630 and retrieve the CARS spectra. The retrieved spectral profiles for the three positions are shown in Fig. 11b, d, and f. The spectral profiles are similar to one another, showing typical spectral profiles of lipids. The reconstructed image is shown in Fig. 11g for the CH bend modes. The spatial inhomogeneity of the O/W emulsion is visualized with a clear vibrational contrast. Note that the intensities in retrieved Im[$\chi^{(3)}$] spectra are proportional to molecular concentrations and therefore the image in Fig. 11g represents the real distribution of the molecules containing the CH bend modes (this is not the case with CARS imaging). We also reconstructed the images for values of $M$, 340 (close to an empirical value, $N$/3), and 750 (an extreme value) shown in Fig 11h and i, respectively. The image contrast for $M$ = 340 looks similar to that for $M$ = 630. It is consistent with Fig. 11a, c, and e, in which the order of pole from 340 to 630 gives a similar value. On the other hand, the artificial spots due to the noise in the spectrum are found in Fig. 11i. Simultaneous measurement of CARS and CSRS provides us with more reliable spectral and spatial molecular information without any arbitrary parameter in the MEM analysis. Although the new technique of MEM is applied to the sample under the electronic nonresonant condition in the present study, a similar approach can also be made for a sample with electronic resonance. As shown in Fig. 7a, the CARS and CSRS signals show intensity difference due to the electronic resonance effect. Therefore, we need to introduce an $M$-independent additional scaling parameter in order to compensate for this intensity difference due to resonance.

## 4. Conclusions

We have developed a simultaneous measurement system of CARS and CSRS. Two unique possibilities are explored. First, the resonance coherent Raman process is investigated. For a β-carotene solution, electronic resonance enhancement differs between the CARS and CSRS processes. Second, combined analysis of the CARS and CSRS spectra leads to a new phase retrieval method in the MEM analysis of coherent Raman spectra. The optimum order of the pole ($M$) can be determined without any arbitrary procedure. This new phase retrieval method is applied to coherent Raman imaging of a model O/W emulsion system (mayonnaise). Using the optimum order, the vibrational image is clearly reconstructed. Simultaneous measurement of CARS and CSRS provides us with more reliable spectral information without any empirical parameter.

## Acknowledgement

This work was supported by the SENTAN project (Program-S) of the Japan Science and Technology Agency (JST). H. Kano gratefully acknowledges financial support by Grand-Aid for Scientific Research on Priority "Molecular Science for Supra Functional Systems" [477] from MEXT, and the Global COE Program for "Chemistry Innovation". The authors thank LEUKOS Company for technical support with the dual-output supercontinuum laser source. The authors gratefully acknowledge Dr. T. Wakisaka, Dr. Y. Masukawa, and Dr. S. Naito (Kao Corporation, Ltd.) for their fruitful discussion. We gratefully acknowledge Mr. J. Ukon (HORIBA, Ltd.) for assisting in the fruitful collaboration between the Japanese and French groups.

## References

[1] G.J. Pupples, F.F.M. De Mul, C. Otto, J. Greve, M. Robert-Nicoud, D.J. Arndt-Jovin, T.M. Jovin, Nature 347 (1990) 301.
[2] A. Zumbusch, G.R. Holtom, X.S. Xie, Phys. Rev. Lett. 82 (1999) 4142.
[3] M. Hashimoto, T. Araki, S. Kawata, Opt. Lett. 25 (2000) 1768.
[4] T.W. Kee, M.T. Cicerone, Opt. Lett. 29 (2004) 2701.
[5] P.R. Carey, Annu. Rev. Phys. Chem. 57 (2006) 527.
[6] H. Kano, H. Hamaguchi, Anal. Chem. 79 (2007) 8967.
[7] C.W. Freudiger, W. Min, B.G. Saar, S. Lu, G.R. Holtom, C. He, J.C. Tsai, J.X. Kang, X.S. Xie, Science 322 (2008) 1857.
[8] Y. Ozeki, K. Itoh, Laser Phys. 49 (2009) 082701.
[9] C.W. Freudiger, M.B.J. Roeffaers, X. Zhang, B.G. Saar, W. Min, X.S. Xie, J. Phys. Chem. B 115 (2011) 5574.
[10] M. Okuno, H. Kano, P. Leproux, V. Couderc, J.P.R. Day, M. Bonn, H. Hamaguchi, Angew. Chem. Int. Ed. 49 (2010) 6773.
[11] M. Okuno, H. Hamaguci, Opt. Lett. 35 (2010) 4096.
[12] P.J. Caspers, G.W. Lucassen, E.A. Carter, H.A. Bruining, G.J. Pupples, J. Invset, Dermatology 116 (2001) 434.
[13] N. Uzunbajakava, A. Lenferink, Y. Kraan, E. Volokhina, G. Vresen, J. Greve, C. Otto, Biophys. J. 84 (2003) 3968.
[14] J.-X. Cheng, X.S. Xie, J. Phys. Chem. B 108 (2004) 827.
[15] Y.-S. Huang, T. Karashima, M. Yamamoto, H. Hamaguchi, Biochemistry 44 (2005) 10009.
[16] B.R. Masters, P.T.C. So, Handbook of Biomedical Nonlinear Optical Microscopy, Oxford University Press, New York, 2008.
[17] J.P. Pezacki, J.A. Blake, D.C. Danielson, D.C. Kennedy, R.K. Lyn, R. Singaravelu, Nat. Chem. Biol. 7 (2011) 137.
[18] K. Bito, M. Okuno, H. Kano, S. Tokuhara, S. Naito, Y. Masukawa, P. Leproux, V. Couderc, H. Hamaguchi, J. Phys. Chem. B 116 (2012) 1452.
[19] J. Nestor, T.G. Spiro, G.K. Klauminzer, PNAS 73 (1976) 3329.
[20] B. Hudson, W. Hetherington III, S. Cramer, I. Chabay, G.K. Klauminzer, PNAS 73 (1976) 3798.
[21] K.P. Dutta, R. Dlinger, T.G. Spiro, J. Chem. Phys. 73 (1980) 3580.
[22] P.R. Carey, Biochemical Applications of Raman and Resonant Raman Spectroscopies, Academic Press, New York, 1982.
[23] H. Kano, H. Hamaguchi, Chem. Lett. 35 (2006) 1124.
[24] H. Kano, H. Hamaguchi, J. Phys. Chem. B 110 (2006) 3102.
[25] W. Min, S. Lu, G.R. Holton, X.S. Xie, Chem. Phys. Chem. 10 (2009) 344.
[26] M.D. Levenson, S.S. Kano, Introduction to Nonlinear Laser Spectroscopy, Academic Press, New York, 1988.
[27] S. Mukamel, Principles of Nonlinear Optical Spectroscopy, Oxford University Press, New York, 1995.
[28] M. Pfeiffer, A. Lau, W. Werncke, J. Raman Spectrosc. 15 (1984) 20.
[29] P.P. Kircheva, J. Raman Spectrosc. 25 (1994) 409.
[30] G.I. Petrov, R. Arora, V.V. Yakovlev, X. Wang, A.V. Sokolov, M.O. Scully, PNAS 104 (2007) 7776.
[31] J.Y. Lee, S.-H. Kim, D.W. Moon, E.S. Lee, Opt. Express 17 (2009) 22281.

[32] K. Isobe, S. Kataoka, R. Mutase, W. Watanabe, T. Higashi, S. Kawakami, S. Matsunaga, K. Fukui, K. Itoh, Opt. Express 12 (2006) 11204.
[33] Y. Wang, C.-Y. Lin, A. Nikolaenko, V. Raghunathan, E.O. Potma, Adv. Opt. Photon. 3 (2011) 1.
[34] A. Volkmer, L.D. Book, X.S. Xie, Appl. Phys. Lett. 80 (2002) 1505.
[35] E.M. Vartiainen, J. Opt. Soc. Am. B 7 (1990) 722.
[36] E.M. Vartiainen, H.A. Rinia, M. Muller, M. Bonn, Opt. Express 14 (2006) 3622.
[37] J.P.R. Day, K.F. Domeke, G. Rago, H. Kano, H. Hamaguchi, E.M. Vartiainen, M. Bonn, J. Phys. Chem. B 115 (2011) 7713.
[38] S. Haykin, Nonlinear methods of Spectral Analysis, Springer-Verlag, New York, 1979.